Volume 16 | Number 3 | 21 January 2014 | Pages 801–1284

PCCP

Physical Chemistry Chemical Physics

www.rsc.org/pccp

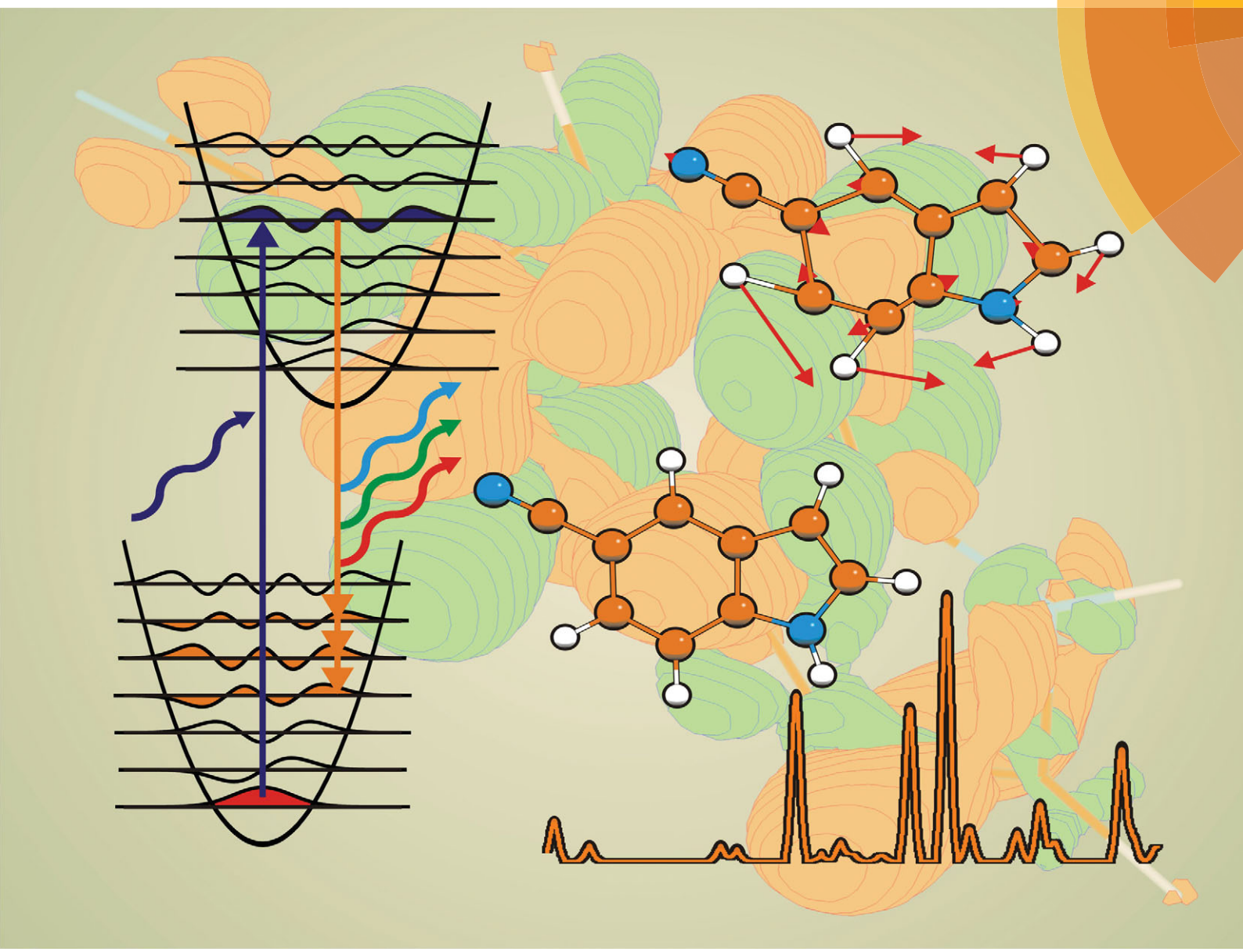

ISSN 1463-9076

ROYAL SOCIETY OF CHEMISTRY

PAPER

Schmitt *et al.*

Determination of the geometry change of 5-cyanoindole upon electronic excitation from a combined Franck–Condon/rotational constants fit

PCCP

PAPER

Determination of the geometry change of 5-cyanoindole upon electronic excitation from a combined Franck–Condon/rotational constants fit†

Cite this: *Phys. Chem. Chem. Phys.*, 2014, **16**, 899

Benjamin Stuhlmann, Anne Gräßle and Michael Schmitt*

Received 27th April 2013,
Accepted 6th September 2013

DOI: 10.1039/c3cp51795k

www.rsc.org/pccp

The geometry change of 5-cyanoindole upon electronic excitation from the ground to the lowest excited singlet state has been determined from a combined fit of the rotational constant changes upon excitation and the vibronic intensities in various fluorescence emission spectra using the Franck–Condon principle. The so determined geometry change is compared to the results of *ab initio* calculations and points to an excited state geometry, which is L_a-like in the nomenclature of Platt. A mode selective coupling of vibronic bands to higher-lying excited states is discussed on the basis of Herzberg–Teller contributions to the Frank–Condon intensities.

1 Introduction

The electronic nature of electronically excited singlet states of substituted indoles has found considerable interest over the last few decades. Most of the studies, which have been performed to unravel the electronic nature of the lowest excited state, rely on methods that determine directly or indirectly the orientation of the transition dipole moment, like two-photon-induced fluorescence anisotropy experiments,[1] two-photon excitation spectroscopy,[2] linear dichroism spectra of partially oriented indole in stretched polyethylene films,[3] and rotationally resolved spectroscopy.[4,5] A different method, which we present here, utilizes the Franck–Condon (FC) factors, in order to determine the geometry changes upon electronic excitation to the state of interest. Comparison of the experimental findings to the results of *ab initio* structure optimizations of the various excited states facilitates the determination of the electronic nature of the excited state. According to the FC principle the probability of a vibronic transition and thus the relative intensity of a vibronic band depends on the overlap integral of the vibrational wave functions of both electronic states. This overlap integral is determined by the relative shift of the two potential energy curves connected by the vibronic transition along the normal coordinates Q of both states. Thus, *via* comparison of measured intensity patterns to the calculated FC factors, the structural change upon electronic excitation can be deduced. Even though the FC principle does not allow for an independent determination of the geometric structure in each of the states, it allows us to enumerate geometry *changes* upon electronic excitation.

Most of the substituted indoles, like indole itself, have the L_b state as a lowest electronically excited state. In some substituted indoles, the L_a/L_b gap is so small, that complex formation with polar molecules like water stabilizes the more polar L_a state so much, that it becomes the lowest electronically excited state. The same effect can be obtained by the introduction of strongly electron withdrawing substituents (like the cyano group) into the 5-position of the chromophore or by electron donating groups (like methyl groups) into the 2 and/or 3-position. Up to now, two substituted indoles have been described in which the L_a state is shifted below the L_b state: 5-cyanoindole[6] and the 2,3-bridged indole derivative tetrahydrocarbazole.[7]

Very few studies of isolated 5-cyanoindole (5CI) in the gas phase have been reported until now. The spectral position and lifetime of the electronic origin of 5CI were determined by Huang and Sulkes using time-correlated single photon counting in a supersonic free jet expansion.[8] Oeltermann *et al.* deduced the structure of 5-cyanoindole in the ground and the lowest electronically excited singlet states using rotationally resolved electronic spectroscopy.[6] Higher vibronic bands of 5CI have been studied by Brand *et al.*[9] While previous studies concentrated on the geometric structures in the different electronic states and the nature of the excited states, we seek to understand the coupling to other electronically excited states in the present contribution.

2 Experimental and computational details

2.1 Experiment

The experimental setup for the dispersed fluorescence (DF) spectroscopy has been described in detail elsewhere.[10,11]

Heinrich-Heine-Universität, Institut für Physikalische Chemie I, D-40225 Düsseldorf, Germany. E-mail: mschmitt@uni-duesseldorf.de; Fax: +49 211 8115195; Tel: +49 211 8112100

† Electronic supplementary information (ESI) available. See DOI: 10.1039/c3cp51795k

In brief, 5-cyanoindole was evaporated at 393 K and co-expanded through a pulsed nozzle with a 500 μm orifice (General Valve) into the vacuum chamber using Helium as carrier gas. The output of a Nd:YAG (Innolas SpitLight 600) pumped dye laser (Lambda-Physik, FL3002) was frequency doubled and crossed at right angles with the molecular beam. The resulting fluorescence was imaged on the entrance slit of a f = 1 m monochromator (Jobin Yvon, grating 2400 lines per mm blazed at 400 nm in first order). The dispersed fluorescence spectrum was recorded using a gated image intensified UV sensitive CCD camera (Flamestar II, LaVision). One image on the CCD chip spectrally covers approximately 600 cm^{-1}. Since the whole spectrum is taken on a shot-to-shot basis, the relative intensities in the DF spectra do not vary with the laser power. The relative intensities are afterwards normalized to the strongest band in the spectrum different from the resonance fluorescence band, which also contains the stray light and is therefore excluded from the FC analysis.

2.2 *Ab initio* calculations

Structure optimizations were performed employing Dunning's correlation consistent polarized valence triple zeta basis set (cc-pVTZ) from the Turbomole library.[12,13] The equilibrium geometries of the electronic ground and the lowest excited singlet states were optimized using the approximate coupled cluster singles and doubles model (CC2) employing the resolution-of-the-identity approximation (RI).[14–16] Spin-component scaling (SCS) modifications to CC2 were taken into account.[17] The Hessians and harmonic vibrational frequencies for both electronic states, which are utilized in the FC fit, have been obtained from numerical second derivatives using the NumForce script[18] implemented in the Turbomole program suite.[19]

2.3 Franck–Condon fit of the structural change

The change in a molecular geometry upon electronic excitation can be determined from the intensities of absorption or emission bands using the FC principle. According to the FC principle the relative intensity of a vibronic band depends on the overlap integral of the vibrational wave functions of both electronic states. The transition dipole moment for a transition between an initial electronic state $|m,v\rangle$ and a final electronic state $|n,w\rangle$ is defined as:

$$M_{vw} = \langle v|\mu_{mn}(Q)|w\rangle \tag{1}$$

with the electronic transition dipole moment $\mu_{mn}(Q)$:

$$\mu_{mn}(Q) = \langle \Psi_m|\mu|\Psi_n\rangle; \quad \mu = \sum_g e r_g \tag{2}$$

where r_g is the position vector of the gth electron. The dependence of the electronic transition dipole moment μ_{mn} on the nuclear coordinates can be approximated by expanding μ_{mn} in a Taylor series about the equilibrium position at Q_0. The series is truncated after the first term in the FC approximation.

The fit has been performed using the program FCFit, which has been developed in our group and described in detail before.[20,21] The program computes the FC integrals of multi-dimensional, harmonic oscillators mainly based on the recursion formula given in the papers of Doktorov, Malkin, and Man'ko.[22,23] and fits the geometry (in linear combinations of selected normal modes) to the experimentally determined intensities. This is simultaneously done for all emission spectra, which are obtained *via* pumping through different S_1 vibronic modes.

The vibrational modes of the electronically excited state can be expressed in terms of the ground state modes using the following linear orthogonal transformation, first given by Duschinsky:[24]

$$Q' = SQ'' + d \tag{3}$$

where Q' and Q'' are the N-dimensional vectors of the normal modes of excited and ground state, respectively, S is a $N \times N$ rotation matrix (the Duschinsky matrix) and d is an N-dimensional vector which displaces the normal coordinates.

The fit of the geometry to the intensities in the vibronic spectra can greatly be improved if independent information for the geometry changes upon electronic excitation is available. This additional information is the change in the rotational constants upon electronic excitation, which can be obtained using rotationally resolved electronic spectroscopy. While geometry fits to the rotational constants (mostly of several isotopologues) are routinely performed using non-linear fits in internal coordinates, the combination of rotational constant changes and vibronic intensities allows for determination of many more geometry parameters.

2.4 Herzberg–Teller corrections to the FC analysis

Truncation of the expansion of μ_{mn} after the second expansion term and inserting into eqn (1) yield the transition dipole moment in the Franck–Condon–Herzberg–Teller (FCHT) approximation:

$$M_{mn} = \mu_{mn}(Q_0)\langle v|w\rangle + \sum_i \left(\frac{\partial \mu_{mn}}{\partial Q_i}\right)_{Q_0} \langle v|Q_i|w\rangle \tag{4}$$

For the evaluation of the Herzberg–Teller (HT) terms $\sum_i \left(\frac{\partial \mu_{mn}}{\partial Q_i}\right)_{Q_0} \langle v|Q_i|w\rangle$ in eqn (4) the partial derivatives of the transition dipole moment with respect to the normal modes must be calculated. These derivatives of μ_{mn} were determined numerically from DFT/MRCI calculations of the respective state using symmetric finite differences:

$$\left(\frac{\partial \mu_{mn}}{\partial Q_i}\right)_{Q_0} = \frac{\mu_{mn}(Q_0 + \Delta Q_i) - \mu_{mn}(Q_0 - \Delta Q_i)}{2\Delta Q_i} \tag{5}$$

The integrals $\langle v|Q_i|w\rangle$ from the HT terms in eqn (4) can be calculated from the FC integrals using the following relation:

$$\begin{aligned}\langle v|Q_i|w\rangle \; = \; & \sqrt{\frac{\hbar}{2\omega_i}}\Big[\sqrt{w_i}\langle v|w_1, \ldots, (w_i - 1), \ldots, w_N\rangle \\ & + \sqrt{w_i + 1}\langle v|w_1, \ldots, (w_i + 1), \ldots, w_N\rangle\Big]\end{aligned} \tag{6}$$

The procedure has been described in detail in ref. 25.

3 Results

3.1 *Ab initio* calculations

The structure of 5CI in its ground and lowest excited singlet states has been determined from an optimization at the spin-component scaled second order coupled cluster (SCS-CC2) level of theory using the cc-pVTZ basis set. The atomic numbering for 5CI, used throughout this publication is shown in Fig. 1. As we have shown in a recent publication on excited states of 5CI,[9] the use of spin-component scaling is mandatory for obtaining the correct order of electronically excited states in this molecule. The Cartesian coordinates of the optimized structures of 5CI in the S_0 and S_1 states are given in the ESI.† 5CI is planar in both electronic states and belongs to the point group C_s.

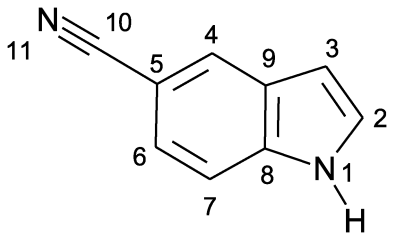

Fig. 1 Atomic numbering of 5CI.

Based on the *ab initio* optimized structures, normal mode analyses of the ground and lowest excited singlet states have been performed at the level of optimization. 5CI has 17 atoms and 45 normal modes, of which 14 are of A″ symmetry and 31 of A′ symmetry. Table 1 summarizes the calculated vibrational frequencies of both electronic states and the largest coefficients

Table 1 Calculated and experimental wavenumbers of the 45 normal modes of the ground and first electronically excited states of 5CI along with the respective symmetries and the coefficients of the Duschinsky matrix, which are larger than 0.3. The wavenumbers of the out-of-plane modes (A″) have been calculated from their first overtones, assuming harmonicity. They are marked with an asterisk

	S_0			S_1			
Mode	Sym.	Calc.	Obs.	Sym.	Calc.	Obs.	Duschinsky
Q_{45}	A″	105.2	100*	A″	77.2	73*	$Q_{45}(S_1) = +0.99Q_{45}(S_0)$
Q_{44}	A′	139.2	140	A′	134.7	138	$Q_{44}(S_1) = +0.99Q_{44}(S_0)$
Q_{43}	A″	225.7	220*	A″	172.1	165*	$Q_{43}(S_1) = +0.99Q_{43}(S_0)$
Q_{42}	A″	263.9		A″	224.3	222*	$Q_{42}(S_1) = +0.98Q_{42}(S_0)$
Q_{41}	A′	379.1	380	A″	308.7	306*	$Q_{41}(S_1) = -0.98Q_{38}(S_0)$
Q_{40}	A″	400.2	410*	A″	334.4	328*	$Q_{40}(S_1) = -0.98Q_{40}(S_0)$
Q_{39}	A′	417.1	416	A′	341.0	350	$Q_{39}(S_1) = -0.87Q_{41}(S_0) - 0.44Q_{39}(S_0)$
Q_{38}	A″	421.3	419*	A″	374.2	365*	$Q_{38}(S_1) = -0.87Q_{37}(S_0) + 0.28Q_{33}(S_0)$
Q_{37}	A″	481.7		A′	394.9	396	$Q_{37}(S_1) = -0.88Q_{39}(S_0) + 0.46Q_{41}(S_0)$
Q_{36}	A′	532.2	536	A′	474.3	484	$Q_{36}(S_1) = -0.88Q_{36}(S_0) - 0.36Q_{34}(S_0)$
Q_{35}	A″	606.1	600*	A″	508.0	508*	$Q_{35}(S_1) = +0.66Q_{33}(S_0) - 0.61Q_{35}(S_0)$
Q_{34}	A′	613.8	613	A″	551.4	545*	$Q_{34}(S_1) = +0.74Q_{35}(S_0) + 0.61Q_{33}(S_0)$
Q_{33}	A″	633.2		A′	582.2	573	$Q_{33}(S_1) = -0.88Q_{34}(S_0) + 0.41Q_{36}(S_0)$
Q_{32}	A″	722.0	710*	A″	599.5		$Q_{32}(S_1) = -0.77Q_{26}(S_0) + 0.42Q_{32}(S_0)$
Q_{31}	A′	729.2	720	A″	615.9		$Q_{31}(S_1) = -0.66Q_{28}(S_0) - 0.55Q_{32}(S_0)$
Q_{30}	A″	758.4		A″	639.1		$Q_{30}(S_1) = -0.71Q_{28}(S_0) + 0.50Q_{32}(S_0)$
Q_{29}	A′	788.2	784	A′	661.6	666	$Q_{29}(S_1) = -0.93Q_{31}(S_0)$
Q_{28}	A″	812.4	812*	A″	689.1		$Q_{28}(S_1) = -0.76Q_{30}(S_0) + 0.37Q_{32}(S_0)$
Q_{27}	A″	853.3		A″	730.8		$Q_{27}(S_1) = +0.97Q_{24}(S_0)$
Q_{26}	A″	896.8		A′	756.8	753	$Q_{26}(S_1) = -0.96Q_{29}(S_0)$
Q_{25}	A′	900.7	900	A″	818.7		$Q_{25}(S_1) = +0.84Q_{27}(S_0) - 0.43Q_{30}$
Q_{24}	A″	934.2		A′	866.9	876	$Q_{24}(S_1) = -0.92Q_{25}(S_0)$
Q_{23}	A′	946.4	944	A′	875.3	884	$Q_{23}(S_1) = +0.90Q_{23}(S_0)$
Q_{22}	A′	1087.9	1070	A′	961.8	951	$Q_{22}(S_1) = +0.41Q_{22}(S_0) + 0.41Q_{18}(S_0)$
Q_{21}	A′	1110.3	1104	A′	1062.8	1065	$Q_{21}(S_1) = -0.75Q_{22}(S_0) + 0.42Q_{21}(S_0)$
Q_{20}	A′	1148.0	1160	A′	1087.1	1095	$Q_{20}(S_1) = +0.73Q_{21}(S_0) - 0.46Q_{20}(S_0)$
Q_{19}	A′	1159.6	1167	A′	1107.3		$Q_{19}(S_1) = -0.84Q_{19}(S_0) - 0.30Q_{22}(S_0)$
Q_{18}	A′	1238.7	1224	A′	1170.5	1158	$Q_{18}(S_1) = -0.68Q_{20}(S_0) + 0.57Q_{18}(S_0)$
Q_{17}	A′	1269.9	1279	A′	1239.0		$Q_{17}(S_1) = +0.91Q_{17}(S_0)$
Q_{16}	A′	1303.8	1318	A′	1272.6		$Q_{16}(S_1) = -0.87Q_{16}(S_0)$
Q_{15}	A′	1353.2	1355	A′	1304.8		$Q_{15}(S_1) = -0.80Q_{15}(S_0) - 0.30Q_{16}(S_0)$
Q_{14}	A′	1390.2		A′	1354.0		$Q_{14}(S_1) = +0.50Q_{14}(S_0) + 0.48Q_{13}(S_0)$
Q_{13}	A′	1457.3	1453	A′	1385.2		$Q_{13}(S_1) = -0.75Q_{12}(S_0) - 0.48Q_{14}(S_0)$
Q_{12}	A′	1487.0		A′	1430.5		$Q_{12}(S_1) = -0.73Q_{11}(S_0) - 0.39Q_{13}(S_0)$
Q_{11}	A′	1499.8		A′	1444.0		$Q_{11}(S_1) = -0.75Q_{10}(S_0) - 0.48Q_{13}(S_0)$
Q_{10}	A′	1546.3	1524	A′	1526.0		$Q_{10}(S_1) = +0.89Q_{9}(S_0) - 0.33Q_{10}(S_0)$
Q_{9}	A′	1611.8	1604	A′	1617.7		$Q_{9}(S_1) = +0.59Q_{14}(S_0) - 0.51Q_{13}(S_0)$
Q_{8}	A′	1657.9	1658	A′	1630.2		$Q_{8}(S_1) = +0.93Q_{8}(S_0)$
Q_{7}	A′	2151.4	2145	A′	2085.1		$Q_{7}(S_1) = -1.00Q_{7}(S_0)$
Q_{6}	A′	3205.8		A′	3218.6		$Q_{6}(S_1) = +0.95Q_{6}(S_0)$
Q_{5}	A′	3214.3		A′	3233.1		$Q_{5}(S_1) = -0.69Q_{5}(S_0) + 0.66Q_{4}(S_0)$
Q_{4}	A′	3226.8		A′	3234.4		$Q_{4}(S_1) = +0.70Q_{5}(S_0) + 0.70Q_{4}(S_0)$
Q_{3}	A′	3267.6		A′	3265.6		$Q_{3}(S_1) = +0.95Q_{3}(S_0)$
Q_{2}	A′	3286.4		A′	3285.1		$Q_{2}(S_1) = -0.95Q_{2}(S_0)$
Q_{1}	A′	3680.4		A′	3672.3		$Q_{1}(S_1) = +1.00Q_{1}(S_0)$

(>0.3) of the Duschinsky matrix *S*. The excited state modes are expressed as linear combinations of the ground state modes with the coefficients given in Table 1. As in other substituted indoles, the Duschinsky matrix is mostly diagonal up to vibrations around 400 cm^{-1} and above 3200 cm^{-1}, for the CH stretching vibrations. Also the CN stretching vibration (Q_7, calculated at 2151.4 cm^{-1}) does not change its vibrational character upon electronic excitation.

No mixing of in-plane and out-of-plane modes occurs, as can be inferred from the last column of Table 1. The complete Duschinsky matrix is given in the ESI.† Additionally, the experimental vibrational frequencies in the S_0 state from the dispersed fluorescence spectra and in the S_1 state from the LIF spectra presented in Section 3.2 are given in Table 1. Since the ground and first electronically excited states of 5CI are of A″ symmetry and the transition dipole moment lies in the plane of the molecule only in-plane (A′) vibrations are allowed. Vibrational wavenumbers of the out-of-plane modes (A″) have been calculated from their first overtones, assuming harmonicity. They have been marked with an asterisk at the respective wavenumber in Table 1.

Compared to indole, 5CI has one more atom, and consequently three additional normal modes. These additional modes are quite local and can be described as in-plane and out-of-plane low frequency wagging modes of the cyano group and as a high frequency CN stretching mode. The lowest frequency mode Q_{45}, which was calculated at 105 cm^{-1} in the electronic ground state, is an out-of-plane wagging motion mostly located in the cyano group. Its frequency strongly drops to 77 cm^{-1} upon electronic excitation. The following vibration Q_{44}, calculated at 139 cm^{-1} (S_0), is the in-plane bending mode of the cyano group, with a slightly reduced frequency in the S_1 state (135 cm^{-1}). The CN stretching vibration is calculated to be 2151 cm^{-1} (S_0) and 2085 cm^{-1} (S_1).

The other normal modes are similar to those of the parent molecule, indole. Q_{43}, calculated at 226 cm^{-1}, represents the butterfly mode of the indole chromophore and is only slightly shifted to the value in indole itself (207 cm^{-1}).[26,27] Q_{42} at 264 cm^{-1} is a ring puckering mode, which is mostly localized in the pyrrole ring. It is observed at 240 cm^{-1} in indole. The in-plane gearing mode of the two rings relative to each other (Q_{41}) is calculated at 379 cm^{-1}. Its S_1 state counterpart (predominately Q_{39}, *cf.* last column in Table 1) is calculated at 341 cm^{-1}. The strongly anharmonic NH out-of-plane mode Q_{40} considerably shifts from 400 cm^{-1} in the ground state to 334 cm^{-1} in the excited state.

3.2 Experimental results

Fig. 2 shows the LIF spectrum of 5CI in the region between the electronic origin and 0,0 + 1200 cm^{-1}. Assignments of the vibronic (S_1) bands are given in Table 1. They are made on the basis of comparison to the frequencies of the *ab initio* calculations and using the propensity rule utilizing the intensities of the respective bands in the fluorescence emission spectra shown in Fig. 3 and in the ESI.†

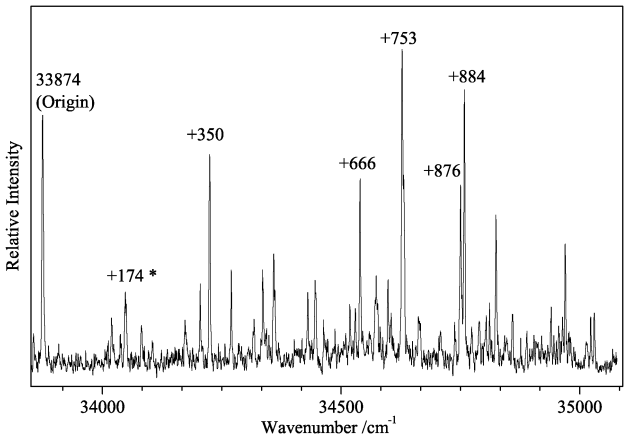

Fig. 2 Laser induced fluorescence spectrum of 5CI. The marked bands at 34 874 cm^{-1} (0,0), 0,0 + 350 cm^{-1}, 0,0 + 666 cm^{-1}, 0,0 + 753 cm^{-1}, 0,0 + 876 cm^{-1}, and 0,0 + 884 cm^{-1} are used for pumping in order to get the DF spectra. The band at 0,0 + 174 cm^{-1} presumably belongs to a 5CI–water cluster.

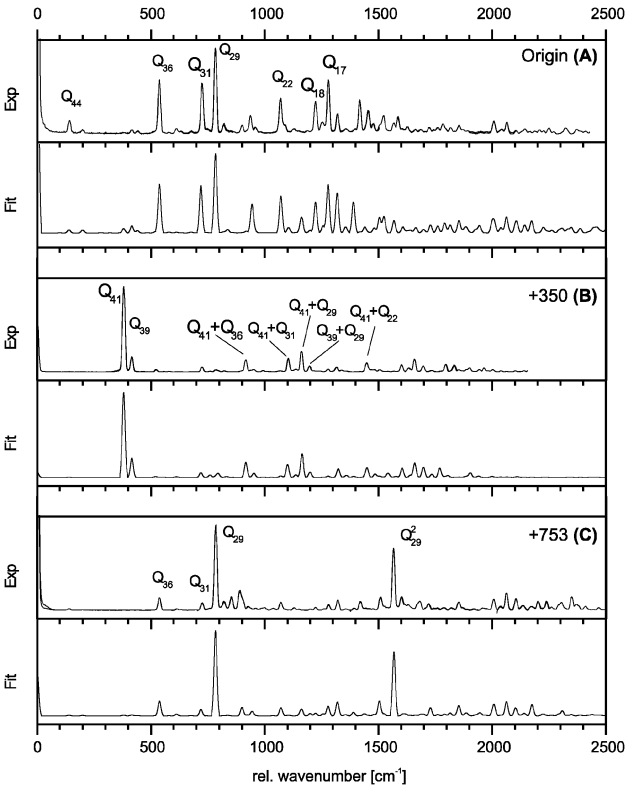

Fig. 3 Dispersed fluorescence spectra of 5CI obtained *via* pumping the electronic origin at 33 874 cm^{-1} (A), *via* the vibronic band at 0,0 + 350 cm^{-1} (B) and *via* the vibronic band at 0,0 + 753 cm^{-1} (C). Within each block, the first trace gives the experimental spectrum, the second trace the FC fit. See the text for details. The wavenumber of each band in the FC fit has been set to the experimental value for better comparison.

Exciting the S_1 band at 350 cm^{-1} leads to an emission spectrum with the strongest propensity to the S_0 band at 380 cm^{-1} (Fig. 3B). The vibronic band is assigned to the vibration Q_{39}, which represents the in-plane gearing mode of the two rings on the basis of its vibrational wavenumber.

According to the Duschinsky matrix, this mode has the largest coefficient at mode Q_{41} in the ground state, leading to a safe assignment of the bands at 380 cm^{-1} (S_0) and 350 cm^{-1} (S_1) to the in plane gearing mode. The emission spectrum is dominated by combination bands of many in-plane vibrations with the diagonal mode Q_{41}, *e.g.* $Q_{41} + Q_{36}$, $Q_{41} + Q_{31}$, and $Q_{41} + Q_{29}$.

The next band whose fluorescence has been dispersed is located at 666 cm^{-1}. It can be assigned to vibration Q_{29}, which has the largest coefficient in the Duschinsky matrix with vibration Q_{31} in the ground state. This is in good agreement with the strongest propensity to the emission band at 720 cm^{-1}. This mode represents a ring breathing mode, mainly localized in the six-ring and the C(5)–C(10) bond. The fluorescence emission spectrum through excitation of the 666 cm^{-1} band along with the simulation and the FC fit is given in the ESI.†

The vibronic band at 753 cm^{-1} leads to an emission spectrum with the strongest propensity to the 784 cm^{-1} mode in the ground state (Fig. 3C). For this vibration, mode Q_{26} in the excited state has the largest coefficient with mode Q_{29} in the ground state. This mode is an in-plane ring deformation mode with major elongations along C(4)–C(9) and N(1)–C(8). Apart from the $Q_{29}|_0^1$ and $Q_{29}|_1^1$ also $Q_{29}|_2^1$ has large intensity.

The vibronic band at 876 cm^{-1} is assigned to mode Q_{24} in the S_1 state, related to mode Q_{24} in the electronic ground state. The respective vibrational energy in the ground state is 935 cm^{-1}. The modes can be described as (in-plane) ring deformations, with main elongations in the pyrrole ring. The fluorescence emission spectrum through excitation of the 876 cm^{-1} band is given in the ESI.† When simulating the LIF spectrum using the best FC fit parameters from all emission spectra (*cf.* Section 3.3) it is obvious that the intensity of the 876 cm^{-1} band is too weak in the simulation (Fig. 5). An alternative assignment of this band could also be based on a Fermi resonance between the combination of Q_{38} (A″) and Q_{35} (A″) with Q_{23} (A′).

Excitation of the energetically close-lying 884 cm^{-1} band leads to an emission spectrum with largest intensity at 944 cm^{-1} (shown in the ESI†). Inspection of the Duschinsky matrix reveals that the S_1 state mode Q_{23} is closely related to the respective Q_{23} band in the electronic ground state. It can be described as in-plane ring deformation, which has its largest elongations at bonds C(3)C(9) and C(4)C(5).

All wavenumbers of the experimentally observed bands both in absorption and in emission, along with the vibrational assignments and their intensities are given in the ESI.†

3.3 FC fit results

The fluorescence intensities in the emission spectra of the electronic origin 0,0 and the vibronic bands at 0,0 + 350 cm^{-1}, 0,0 + 666 cm^{-1}, 0,0 + 753 cm^{-1}, and 0,0 + 884 cm^{-1} have been utilized along with the rotational constants of 5CI in the ground and lowest excited states from ref. 6 in the fit of the geometry changes upon electronic excitation. We employed a weighting factor of 5 for the fit of the rotational constants and of 1 for the fit of the fluorescence intensities. Inspection of the DF spectrum of the electronic origin (Fig. 3A) shows that all vibrational bands in the fit of the FC emission spectrum *via* pumping the electronic origin are well reproduced. Also the fluorescence emission spectra though 0,0 + 350 cm^{-1} (3B), 0,0 + 753 cm^{-1} (3C) and 0,0 + 666 cm^{-1} (shown in the ESI†) are nearly perfectly reproduced by the FC fit. Strong deviations are found for the two emission spectra through 0,0 + 876 and 0,0 + 884 cm^{-1} (shown in the ESI†). The vibrational modes, which are used to model the geometry changes upon electronic excitation are compiled in Table 2 along with the magnitude and sign of their displacements.

Table 2 Fitted factors of the displacements along the normal modes from the FC fit

Mode	Displacement
Q_{36}	0.032325 ± 0.0071828
Q_{31}	0.0031924 ± 0.0031209
Q_{29}	0.0010253 ± 0.0022252
Q_{25}	−0.039721 ± 0.0072168
Q_{22}	−0.042237 ± 0.015752
Q_{18}	0.015171 ± 0.016185
Q_{17}	0.10041 ± 0.012041

Table 3 summarizes the results for the geometry changes from the combined fit to the rovibronic intensities and the rotational constant changes upon electronic excitation from ref. 6. While in the SCS-CC2 calculations, there are slight discrepancies in the description of the rotational constants, especially for the change in the *A* rotational constant upon electronic excitation, the combined fit perfectly reproduces all rotational constant changes upon electronic excitation. The intensities in the fluorescence emission spectra through the origin and the vibronic bands at 0,0 + 350, 0,0 + 666, and 0,0 + 753 cm^{-1} are perfectly reproduced, while the emission spectra through the 0,0 + 876 cm^{-1}, and 0,0 + 884 cm^{-1} bands show strong deviations from the FC fit.

Fig. 4 depicts the results of the structure fit to the rotational constants and the FC intensities graphically.

Table 3 Rotational constants, their changes upon electronic excitation, and bond lengths of 5CI in the electronic ground and lowest excited singlet states from SCS-CC2 calculations utilizing the cc-pVTZ basis set and from a FC fit. The reference state for the geometry changes is the electronic ground state. Therefore, the geometry parameters for the ground state in the FC fit have been taken from the SCS-CC2 calculations. For atomic numbering *cf.* Fig. 1

State	S_0		S_1		$S_1 - S_0$		
method	SCS-CC2	FCFit	SCS-CC2	FCFit	SCS-CC2	FCFit	Exp.[6]
A	3364	3364	3281	3293	−83	−70.50	−70.47
B	734	734	725	726	−9	−7.83	−7.69
C	602	602	594	595	−6	−7.54	−7.37
N1C2	138.3	138.3	138.3	139.6	0	+1.3	—
C2C3	137.3	137.3	139.4	139.0	+2.1	+1.7	—
C3C9	143.5	143.5	141.4	141.6	−2.1	−1.9	—
C9C4	140.3	140.3	141.9	142.9	+1.6	+2.6	—
C4C5	139.4	139.4	144.2	144.3	+4.8	+4.9	—
C5C6	141.8	141.8	144.8	145.0	+3.0	+3.2	—
C6C7	138.6	138.6	142.0	141.2	+3.4	+2.6	—
C7C8	140.1	140.1	140.7	139.3	+0.6	−0.8	—
C8C9	142.2	142.2	146.2	145.2	+4.0	+3.0	—
C8N1	137.5	137.5	138.1	138.6	+0.6	+1.1	—
N1H12	100.5	100.5	100.5	100.6	0	+0.1	—
C5C10	143.7	143.7	141.6	140.9	−2.1	−2.8	—
C10N11	117.6	117.6	118.2	118.0	+0.6	+0.4	—

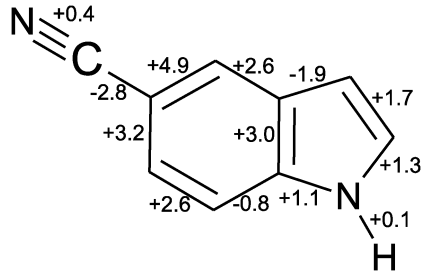

Fig. 4 Geometry changes of 5CI upon electronic excitation from a combined FC/rotational constants fit. The numbers give the bond length changes in pm upon excitation from the ground state to the lowest electronically excited state.

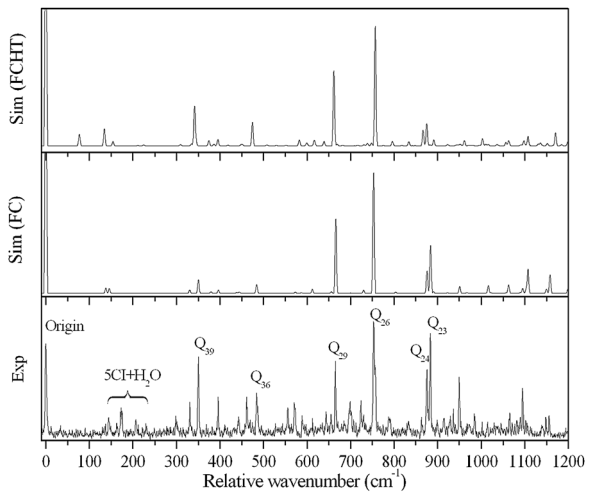

Fig. 5 Laser induced fluorescence spectrum of 5CI along with a simulation using the structural changes from the FC fit and a simulation with additional Herzberg–Teller corrections.

On the basis of the structural changes fit in this way, we calculated the LIF spectrum of 5CI using the FC approximation. Fig. 5 shows the LIF spectrum of 5CI along with a FC simulation of the absorption spectrum using the geometry changes from the FC fit of the emission spectra, described above. Most intensities of the vibronic spectrum are quite well reproduced, with the exception of the intensity of the bands at 350, 876, and 884 cm^{-1}, which are considerably too weak. Using the geometry changes from the FC fit we implemented additional corrections from the Herzberg–Teller terms, calculated using the numerical derivatives of the DFT/MRCI transition dipole moments along the normal modes as described in Section 2.4. Most of the intensities, which are missing or weak in the FC simulation of the absorption spectrum, are considerably improved in the FCHT simulation. Exceptions are the bands at 876 and 884 cm^{-1}, which also show large deviations in the FC fit of the emission spectra.

4 Conclusions

The geometry changes, which have been determined from the FC analysis, point to a structure of the excited state, which is L_a like in the nomenclature of Platt. Especially the strong elongations along the CC bonds C(2)–C(3), C(5)–C(6) and C(8)–C(9) are typical for the structure in this electronic state. Thus, the structure in the excited state, determined *via* the FC analysis, fully confirms the findings from the analysis of the direction of the transition dipole moment.[6] Like in tetrahydrocarbazole (THC),[7] the lowest, optically bright state is of L_a character. While in the latter case the reason for the low-lying L_a state can be found in the positive inductive (+I) effect of the ethyl bridge, between positions 2 and 3 of the pyrrole ring, in 5CI it is the strong negative mesomeric effect of the cyano group in the 5-position of the benzene moiety.

The assignment of S_1 state (L_a) transitions to the respective ground state modes is straightforward in this molecule. Like in THC, the Duschinsky matrix is predominately diagonal (*cf.* Fig. 6), in contrast to the case of indole, in which the Duschinsky matrix is severely perturbed, and projection of the excited state modes onto specific ground state vibrations is difficult. Strong deviations from diagonal behavior in indole is found for vibrational quantum number ranges, which strongly couple to the higher lying L_a state that induces strong Herzberg–Teller perturbations in the vibronic spectrum of the L_b state. In both 5CI and THC the lower state with higher oscillator strength is the L_a state, with L_b being more than 1200 cm^{-1} higher in energy.

Mode selective perturbations are found for vibronic bands Q_{39} at 350 cm^{-1} Q_{24} at 876 cm^{-1}, and Q_{23} 884 cm^{-1}. While the FC intensities of the emission through all other vibronic bands are perfectly matched, the modes Q_{24} and Q_{23} show strong deviations, both in absorption and in emission, while deviations of the 350 cm^{-1} band are limited to the absorption spectrum. Based on the direction of the transition dipole moments it was previously concluded that these bands strongly couple to the higher-lying L_b state *via* Herzberg–Teller

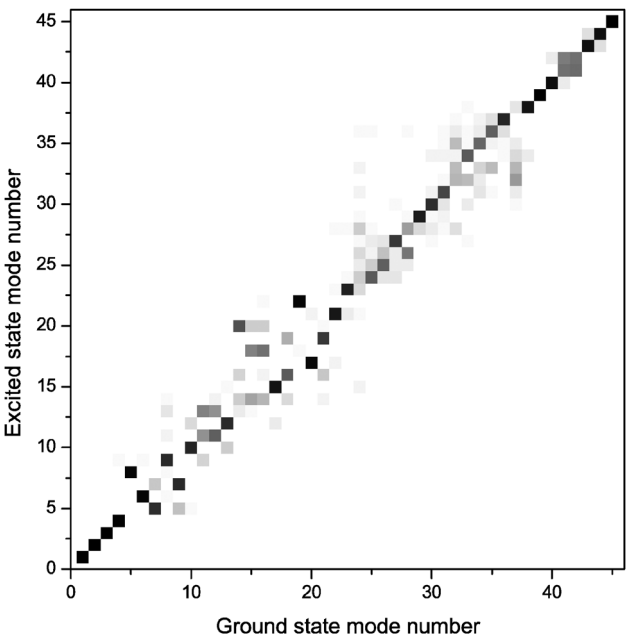

Fig. 6 Graphical representation of the 45 × 45 Duschinsky matrix of 5CI, calculated using the numerically determined Hessian at the SCS-CC2/cc-pVTZ optimized structures.

coupling.[9] The Duschinsky matrix is nearly diagonal for these modes, excluding strong mode mixing to be responsible for the observed deviations. While our Herzberg–Teller analysis shows that the intensity of the 350 cm^{-1} band can be explained by the additional contributions from the HT terms in eqn (4), the deviations of the bands at 875 and 884 cm^{-1} cannot be explained on the basis of Herzberg–Teller contributions to the FC spectrum. Our FC analysis, presented here of the 5CI spectra showed that excitation to the L_a state leads to an increased NH bond length. The energy of the repulsive $\pi\sigma^*$ state decreases with increasing NH bond length as deduced from CASPT2 potential energy profiles along the NH coordinate by Sobolewski *et al.*[28] It seems therefore plausible to postulate an intersection with the $\pi\sigma^*$ state approximately 900 cm^{-1} above the adiabatic L_a origin to be responsible for the non-FC and non-HT behavior in the absorption and emission spectra of 5CI. The longer NH bond length in the S_1 state is in agreement with a decrease of the pK_a value upon excitation to the lowest excited singlet state as known for the indoles. Using the absorption maxima of 5CI and of its anion from ref. 29 and the relation from the Förster cycle:[30]

$$\Delta \mathrm{p}K_a = \frac{hc(\tilde{\nu}_{HA} - \tilde{\nu}_{A^-})}{2.303 k_B T} \quad (7)$$

where $hc\bar{\nu}_{HA}$ and $hc\bar{\nu}_{A^-}$ are the wavenumber of the 5CI absorption maximum and of its anion, respectively, we calculated the change in the pK_a of 5CI to be −6.0 in agreement with the increased NH bond length upon excitation.

Acknowledgements

The authors like to thank the Universitätsrechenzentrum Köln for the granted computing time on Cheops. The financial support from the Deutsche Forschungsgemeinschaft (SCHM 1043/12) is gratefully acknowledged.

References

1 P. R. Callis, *Topics in Fluorescence Spectroscopy*, Plenum Press, New York, 1977, vol. 5, pp. 1–42.
2 D. M. Sammeth, S. Yan, L. H. Spangler and P. R. Callis, *J. Phys. Chem.*, 1990, **94**, 7340–7342.
3 B. Albinsson and B. Nordén, *J. Phys. Chem.*, 1992, **96**, 6204.
4 C. Brand, J. Küpper, D. W. Pratt, W. L. Meerts, D. Krügler, J. Tatchen and M. Schmitt, *Phys. Chem. Chem. Phys.*, 2010, **12**, 4968–4997.
5 J. Küpper, D. W. Pratt, W. L. Meerts, C. Brand, J. Tatchen and M. Schmitt, *Phys. Chem. Chem. Phys.*, 2010, **12**, 4980–4988.
6 O. Oeltermann, C. Brand, B. Engels, J. Tatchen and M. Schmitt, *Phys. Chem. Chem. Phys.*, 2012, **14**, 10266–10270.
7 O. Oeltermann, C. Brand, W. L. Meerts, J. Tatchen and M. Schmitt, *J. Mol. Struct.*, 2011, **933**, 2–8.
8 Y. Huang and M. Sulkes, *Chem. Phys. Lett.*, 1996, **254**, 242–248.
9 C. Brand, B. Happe, O. Oeltermann, M. Wilke and M. Schmitt, *J. Mol. Struct.*, 2013, **1044**, 21–25.
10 M. Schmitt, U. Henrichs, H. Müller and K. Kleinermanns, *J. Chem. Phys.*, 1995, **103**, 9918–9928.
11 W. Roth, C. Jacoby, A. Westphal and M. Schmitt, *J. Phys. Chem. A*, 1998, **102**, 3048–3059.
12 R. Ahlrichs, M. Bär, M. Häser, H. Horn and C. Kölmel, *Chem. Phys. Lett.*, 1989, **162**, 165–169.
13 J. T. H. Dunning, *J. Chem. Phys.*, 1989, **90**, 1007–1023.
14 C. Hättig and F. Weigend, *J. Chem. Phys.*, 2000, **113**, 5154–5161.
15 C. Hättig and A. Köhn, *J. Chem. Phys.*, 2002, **117**, 6939–6951.
16 C. Hättig, *J. Chem. Phys.*, 2002, **118**, 7751–7761.
17 A. Hellweg, S. Grün and C. Hättig, *Phys. Chem. Chem. Phys.*, 2008, **10**, 1159–1169.
18 P. Deglmann, F. Furche and R. Ahlrichs, *Chem. Phys. Lett.*, 2002, **362**, 511–518.
19 *TURBOMOLE V6.3 2012, a development of University of Karlsruhe and Forschungszentrum Karlsruhe GmbH, 1989-2007, TURBOMOLE GmbH, since 2007; available from* http://www.turbomole.com.
20 D. Spangenberg, P. Imhof and K. Kleinermanns, *Phys. Chem. Chem. Phys.*, 2003, **5**, 2505–2514.
21 R. Brause, M. Schmitt, D. Spangenberg and K. Kleinermanns, *Mol. Phys.*, 2004, **102**, 1615–1623.
22 E. V. Doktorov, I. A. Malkin and V. I. Man'ko, *J. Mol. Spectrosc.*, 1975, **56**, 1–20.
23 E. V. Doktorov, I. A. Malkin and V. I. Man'ko, *J. Mol. Spectrosc.*, 1977, **64**, 302–326.
24 F. Duschinsky, *Acta Physicochim. URSS*, 1937, **7**, 551–577.
25 M. Böhm, J. Tatchen, D. Krügler, K. Kleinermanns, M. G. D. Nix, T. A. LeGreve, T. S. Zwier and M. Schmitt, *J. Phys. Chem. A*, 2009, **113**, 2456–2466.
26 T. L. Smithson, R. A. Shaw and H. Wieser, *J. Chem. Phys.*, 1984, **81**, 4281–4287.
27 G. A. Bickel, D. R. Demmer, E. A. Outhouse and S. C. Wallace, *J. Chem. Phys.*, 1989, **91**, 6013.
28 A. L. Sobolewski, W. Domcke, C. Dedonder-Lardeux and C. Jouvet, *Phys. Chem. Chem. Phys.*, 2002, **4**, 1093–1100.
29 G. Yagil, *J. Phys. Chem.*, 1967, **71**, 1034–1044.
30 A. Weller, *Z. Elektrochem.*, 1952, **56**, 662–668.